Environmental Engineering and Management Journal

August 2020, Vol.19, No. 8, 1427-1442
http://www.eemj.icpm.tuiasi.ro/; http://www.eemj.eu

"Gheorghe Asachi" Technical University of Iasi, Romania

TURBULENT FLOW CHARACTERISTICS IN THE ERODED REGION OF THE SIDE-WALL BANK

Krishnendu Barman[1*], Pankaj Kumar Raushan[2], Vikas Kumar Das[2], Sayahnya Roy[2], Sunil Hansda[2], Koustuv Debnath[2]

[1]Applied Mathematics with Oceanology and Computer Programming, Vidyasagar University, Paschim Medinipur 721102, West Bengal, India
[2]Department of Aerospace Engineering and Applied Mechanics, Indian Institute of Engineering Science and Technology (IIEST), Shibpur 711103, India

Abstract

An experimental inquest was performed to quantify the turbulent flow characteristics near the eroded region of an artificial side-wall bank at three different flow depths, and a comparison study is made between before and after erosion for two Reynolds numbers. Instantaneous flow velocities were taken with an acoustic Doppler velocimeter (ADV) at near bank of the vertical side wall. The mean flows and other turbulence quantities such as Reynolds shear stress, turbulent intensities, and turbulent kinetic energy for two Reynolds numbers are discussed. Turbulence strength (Reynolds shear stress and turbulent intensities) are maximum at the eroded region of bank wall. The paper described the fractional contributions of ejection-sweep cycles to the stress and timescale of occurrence of ejection-sweep events at the eroded region. The probability density function of the velocity fluctuations provides information on the direction of the transportation of the turbulent energy, which is responsible for removal of bank material.

Key words: bank erosion, bursting events**,** cohesive sediments, Reynolds shear stress, turbulence

Received: July, 2019; Revised final: February, 2020; Accepted: April, 2020; Published in final edited form: August, 2020

1. Introduction

The river bank erosion is the most concern for many engineers, scientists, geologist, and civilians. Many types of research are going on to understand river bank erosion mechanism and flow characteristics near the bank region. Turbulent flow phenomenon is important to understand sediment erosion, transport, and hydraulic processes. Turbulence can be seen in many ways in nature, and it has large applications in the environmental engineering science, rivers, and coastal regions to identify soiled solutes and sediments (Rutherford, 1994), fish habitat depiction (Katopodis, 1996). Turbulent characteristics in a boundary layer play an imperative responsibility in sediment transport and bedform development (Best, 1993). A classical study is the identification of coherent structure in the bottom-wall region, scoured region and eroded region of a vertical side wall in turbulent flow (Grass, 1971).

Previous researchers studied and conducted experimental work using flume (Meijer and Van Velzen, 1999). Prior work (Nezu and Onitsuka, 2001) measured the turbulence in channel flows over the vegetated cover bed; and observed the horizontal vortices at the free surface. They also concluded that the turbulence was transported by secondary current laterally near the zone of non-vegetation to vegetation. The characterization property of river bed and bank condition performed significant importance to understand the turbulent flow characteristics near the bank region. In alluvial channels, water penetrates the bed and side banks in the process of seepage. The porosity of sediment particles in the stream and groundwater level plays an active role on the

* Author to whom all correspondence should be addressed: e-mail: krishnendubarman07@gmail.com; Phone: +91 8777809557

penetration of water into river channel and streams. The occupancy of downward seepage assists to enhance sediment transport and bed shear stress which possibly changes the hydrodynamic features of the channel (Cao and Chiew, 2014; Rao and Sitaram, 1999; Rao et al., 2011). Experimental study (Maclean and Willets, 1986) on a river absorption system observed that the bed shear stress increases due to suction at the bottom wall, whereas similar observation was also spotted in other studies by (Cao and Chiew, 2014; Chen and Chiew, 2004; Maclean, 1991; Singha et al., 2012) signifying the progress of uniform velocity profile. To ensure the control flow condition for sustaining food-web and improving navigational flow depth in natural rivers, aquatic vegetation is an essential part of such effort (Huai et al., 2019a, b). Further, Huai et al. (2019a, b) performed an experimental study on turbulent flow structure over submerged vegetation and showed that the momentum flux convey through sweep is greater around the canopy bottom wall.

Several theoretical studies have been addressed for understanding the mechanisms driving channel widening and formation of the eroded region on the vertical side wall have been addressed in the literature. Flume studies provide the benefit of a controlled experimental background with isolated hydraulic forces and channel response (Thompson and Wohl, 1998). The hydraulic behavior is also important for driving channel widening, and it happens due to the shear-layer effect. Changes in velocity along the main channel and floodplain flow formed a shear layer at the interface between main channel and floodplain flow (Shiono and Knight, 1991; Wormleaton, 1996). These shear layers are comprise of periodic and form a whirlpool-like flow structure often known as vortices or coherent structures (Smith, 1996; Tritton, 1988).The hydraulic characteristics of near bank flow consist with vertical side wall along eroded regions thus the impact of bank morphologies is a major reason for turbulent flow near the bank region. Another reason may be possible due to the formation of the irregular eroded cavity on the vertical side wall and channel widening which incur the hydraulic effect near bank region flows.

To the authors knowledge, it is required more precisely enlighten about the turbulent flow characteristic near the bank region and measure the turbulence which affects the vertical side bank wall. Also, the change of flow characteristic is important after certain erosion as it forms a cavity into the bank wall under different hydraulic condition. The study, specifically about the turbulent flow characteristics near the bank wall as well as eroded region of the bank in various hydraulic conditions, has not been yet addressed in the literature. This study explores how the turbulence characteristics are changed in non-eroded region (NER) and eroded region (ER) of the vertical bank. Results provide the turbulence flow characteristics, such as time-averaged velocities, turbulent intensities and Reynolds shear stresses along a stream-wise direction at different flow depths for two Reynolds numbers. The paper also contains the variation of normalized turbulent kinetic energy in three eroded regions for different flow depths. The fractional contribution to total shear stress and occurrence of time scale for ejection-sweep cycles are shown for eroded and non-eroded region. This experimental results are useful for better understanding of the near bank turbulence effect on the river flow that are solely responsible for cohesive sediment erosion and widening of the channel under different hydraulic condition.

2. Material and methodology

2.1. Experimental setup

A series of experiments were conducted in a specially designed laboratory flume at the Fluid Mechanics and Hydraulic Laboratory (FMHL) of the Indian Institute of Engineering Science and Technology (IIEST), Shibpur, India. The experimental flume (Fig. 1) has dimensions of 18 m length, 0.6 m width and 0.9 m height. An adjustable tailgate was used at the end of the flume to get desired water depth and flow velocity for maintaining subcritical flow. The subcritical flow defined by the Froude number (Fr), when $Fr<1$ and its expression was $F_r = U/\sqrt{gh}$, where U, g and h are mean flow velocity, gravitational acceleration and water depth, respectively. In the present study F_{r1} = 0.456 and F_{r2} = 0.651 for the Reynolds number, R_{e1}=168000 and R_{e2} = 240000 respectively. The Reynolds number calculated from the expression, $R_e = Uh/\nu$ in which ν is kinematic viscosity.

Three-dimensional (3-D) instantaneous velocity components were measured with a SonTek side-looking 16-MHz micro acoustic Doppler velocimeter (ADV). The sampling volume of the ADV is of a cylindrical shape of dimension 0.3 cm in radius and 0.32 cm in length. Thus, according to Barman et al. (2019a) the minimum distance required for the ADV measurement at near wall is 0.4 cm. It may be noted that in the present experiment the normalised location (normalised by water depth, h) of the near wall ADV measurement is 0.4/24 = 0.02. Further, an underwater camera was used to record the formation of pitting structures and the undercut development. Furthermore, a depth gauge was used to measure the dimensions of the undercut observed.

2.2. Bed preparation technique

The cohesive sediments used as a part of the investigations were collected from the lower course of river Ganges (Hooghly River) in India. Particle size analysis of the River Ganges sediment was carried out using a Malvern particle size analyzer (Laser Diffraction method) shown in Table 1. For the sediment collected from the bank of river Ganges, the dry cohesive lumpy material (mainly clay) was powdered manually using a 4-kg compacting ground

rammer with base diameter of 0.1 m and then was passed through 5 mm diameter sieve to eliminate any unwanted materials and to ensure evenness of the grain size (it was done to remove any organic matter or detritus as it influences the cohesion within the cohesive sediment structure. Water by weight in one-hundredth of dry material was added to the sediment in a vessel and blended rigorously to acquire appropriate consistency. The mixture was then allowed to go through a 5 mm sieve to confirm uniform blending.

Bank material was mixed properly before it packing into the sediment recess. The cohesive mixture was filled approximately 0.05 m in layers into the test channel and compacted by dynamic compaction (Debnath and Chaudhuri, 2010).

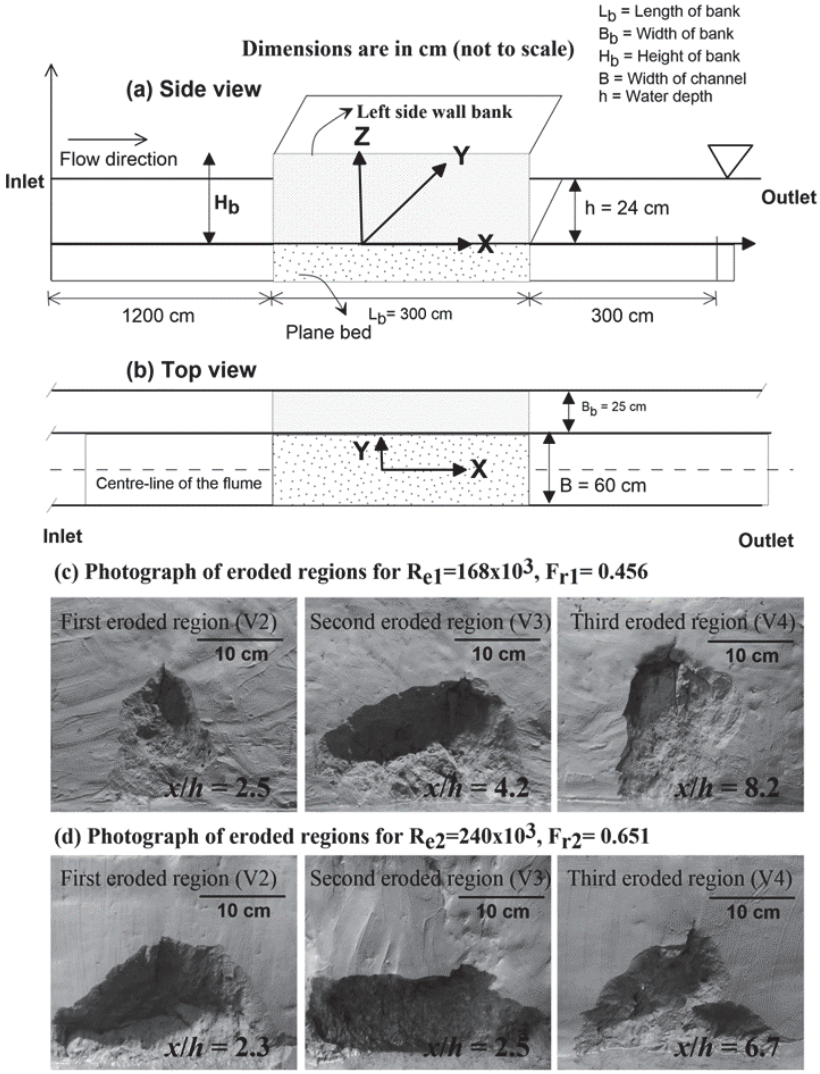

Fig. 1. (a, b) represents the front and top view of schematic diagram of flume set-upshown with vertical side wall and (c, d) shows the photographof eroded region near bank for both Reynolds numbers

Table 1. Properties of the different sediment used in the experiments

Properties	***River Ganges Sediment (RGS)***
Specific Gravity	2.66
d < 4μm	25.64%
4μm< d ≤ 63μm	66.15%
d > 63μm	8.21%
Median Size	16.72 μm
LL	37.39%
PL	24%
PI	17.61%
Maximum dry unit weight	1.85 g/cm^3
OMC	21%
τ_s at optimum moisture content	14.77 kN/m^2

LL-Liquid Limit; PL- Plastic Limit; PI- Plasticity Index; OMC- Optimum moisture content

After that, a wooden plank was placed and holds tightly using five *L*-shaped clamps with existing flume side wall. Following this procedure, a rectangular cast cohesive bank of length 3 m was made at the left side of the flume. Similar process was repeated similar to bed preparation technique for the preparation of the artificial side bank. The dimension of an artificial bank prepared was of length 300 cm, width 25 cm, and height 40 cm.

2.3. Experimental procedure

The test section was located at 10 m from the inlet of the flume, where the detailed measurements were taken. The water depth was kept constant at h = 24 cm for experimental runs. The schematic diagrams of experimental setup and the locations of eroded regions are shown in Fig. 1. The experimental runs were performed for both Reynolds numbers $R_e = 168\times10^3$ and 240×10^3. A coordinate system shown in Fig. 1 (a) where the x = 0 represents the starting point of the artificially prepared bank from the upstream of the flume. In Fig. 1 (a), the coordinate y = 0 is designated as bank wall before erosion and the depth of undercut designated as positive y direction where z = 0 represents the origin of bank height. Total duration of the experiments was carried out for 240 hrs for both Reynolds number cases. Visual and photographic observation showed that the initial erosion rate was high, which gradually decreased with increase in time. Further, the dislodgment of the sediment particles from the bank face was negligible and reached nearly stable condition after 120 hours. Thus, the experiments were conducted for another 120 hrs after which the velocity measurements were conducted. Firstly, the velocity measurements were carried at non-eroded condition at z/h = 0.5. Furthermore, after the initiation of the erosion and formation of the undercut, velocity measurements were deployed at 20 locations in the stream-wise direction for three different flow depths. The measurement were taken close to the bank face (i.e. 0.4 cm, y/h = 0.02) within the eroded region and on non-eroded region as well. Dimensions of the undercut formed for both Reynolds numbers at three different locations are shown in Table 2 while the hydraulic conditions and bank specification are given in Table 3. It is worthwhile to mention here that in the present experimental condition different flow conditions are considered as in the natural river channel where the discharge of the river varies due to seasonal variation. This variation in the river channel is mainly caused during heavy rainfall and results in an increased flow velocity. Thus, in the present experiments two different flow cases have been tested.

3-D velocity components were measured near the bank along the stream-wise direction at a different location before the erosion and after the erosion for both Reynolds numbers. Micro-acoustic Doppler velocimeter (ADV) was used for measuring the turbulent velocity for 180 s at a sampling rate of 40 Hz to ensure full characterization of turbulent flow. The sampling volume size is 0.09 cm^3 and calibration of ADV is bound to be ±1.0% of taken velocity. Further, accuracy for 100 cm/sec velocity data is ±1 cm/s. The detailed descriptions of ADV are provided in previous work (Barman et al., 2016; Debnath et al., 2012). The signal strength of velocity components and correlations are used primarily to determine the quality and accuracy of the velocity data measured by ADV. The "raw" ADV velocity components data are evidenced by high levels of noise and spikes (Nikora and Goring, 1998). In turbulent flows, the ADV velocity fluctuations characterize the combined effects of the Doppler noise, signal aliasing, velocity fluctuations, installation constraints and other disturbances. The sensitivity analyses were performed on ADV data in turbulent flow. Primarily the data set was "cleaned" by excluding low-correlation (<70%) and low signal-to-noise ratio (<15) samples, and by removing "spikes" using a phase-space threshold technique (Goring and Nikora, 2002). This stage was performed by Win ADV software package.

Assessment of uncertainty of turbulence parameters is essential to quantify the quality for measuring data. Statistical uncertainty occurred due to constraint of measurement device and also the boundary conditions.

Table 2. Dimensions of the eroded bank face for the different locations

Undercut location	***First eroded region***			***Second eroded region***			***Third eroded region***		
	L (cm)	*H*(cm)	*D* (cm)	*L* (cm)	*H*(cm)	*D* (cm)	*L* (cm)	*H*(cm)	*D* (cm)
R_{e1}	18.70	20.78	2.80	41.50	19.30	7.20	19.70	22.10	3.40
R_{e2}	47.00	21.10	10.80	48.00	16.60	8.40	42.30	21.57	4.90

R_e= Reynolds number; L, H and D = Length, height and depth of the undercut dimension

Table 3. Hydraulic parameters

Run	***Free-stream mean velocity*** (U_o)	***Channel width (B)***	***Water depth (h)***	***Discharge*** (Q)	***Reynolds numbers (R_e)***	***Bank specification and dimensions***		
						Length of bank	***Width of bank***	***Height of bank***
1	70 cm/sec	60 cm	24 cm	100.80 m^3/s	168000	300 cm	25 cm	40 cm
2	100 cm/sec	60 cm	24 cm	144.00 m^3/s	240000	300 cm	25 cm	40 cm

The relation of standard error for mean and variance of measuring data as Eqs. (1- 2) (Garcia et al., 2006; Hansda et al., 2019):

$$\zeta^2_{\text{mean}} = \zeta^2_u / N_{\text{meaneff}} \quad (1)$$

$$\zeta^2_{\text{var}} = 2(\zeta^2_u)^2 / N_{\text{vareff}} \quad (2)$$

Here ζ^2_u signify the sample variance of u; $N_{\text{meaneff}} = T_t / 2T_s$ and $N_{\text{vareff}} = T_t / T_s$ are the effective sample sizes for the mean and variance where T_t and T_s represents the total sampling time and integral time scale for autocorrelation procedure. To formulate the standard errors of the turbulence parameters, the moving block bootstrap (MBB) method is used while the confidence interval was found nearly 95% for a particular signal. The synthetic data sets were prepared using MBB method for each 150 s time series stream-wise velocity data between the interval (50 cm/s ≤ u ≤ 120 cm/s). The MBB technique was synthesized by 1000 replications for each 180 s time signal. A comparison study of standard error for sample mean and variance of functioned data (acquired by MBB method) and experimental data are shown in Fig. 2 (a, b). A significant similarity was observed among MBB and following equations to calculate the errors. The error values for the turbulence parameters are taken nearly 12% for the present study. Particularly, the standard error of sample mean and variance were obtained nearly 3.2% and 10.4% respectively. Further, Fig. 2c reveals that the effects of the sample size considered for analysis of turbulence characterisation near the vertical bank. In the Fig. 2c, errors of standard deviation of stream-wise velocity component are shown for two Reynolds number cases. The sampling location was taken at 3.5 cm above the bed near the bank region as an example. The stream-wise velocity statistical properties were most sensitive to the number of data points per sample (Chanson et al., 2007). The statistical moments, mean and standard deviations, were adversely affected by sampling durations less than 100s or less than 5000 samples. Also, they demonstrated that in steady open channel flows, the sampling record must be larger than 5000 samples to yield minimum errors on first and second statistical moments of the velocity components. In the present study 7000 samples are enough for statistical measure.

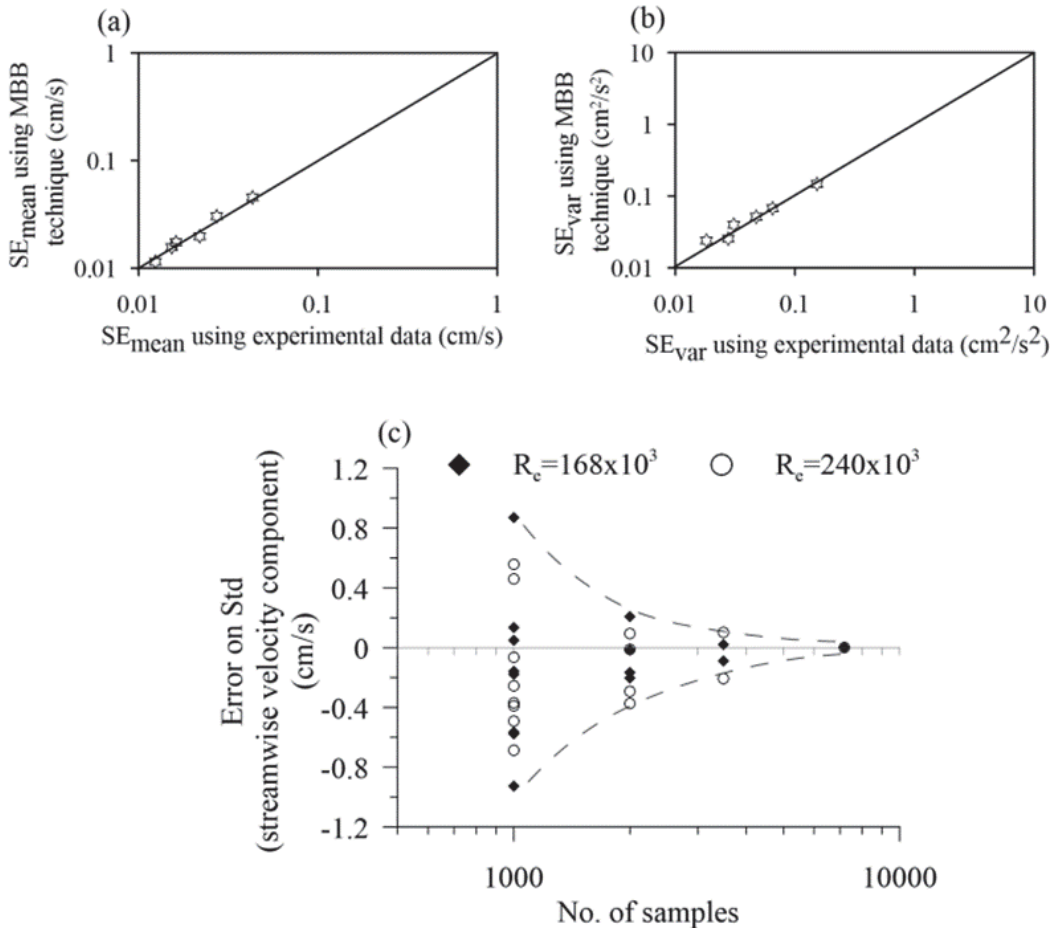

Fig. 2. Comparison between standard errors of the sample (a) mean and (b) variance computed for each signal using MBB technique with respect to Eqs. (1-2); (c) effect of data sample size on turbulent flow velocity component in a flume where flow parameters: R_e= 168000 and 240000, channel width = 0.6 m, water depth = 0.24 m, 16 MHz micro-ADV instrument, sampling rate = 40 Hz

3. Results and discussion

Here, (*u, v, w*) denotes the instantaneous stream-wise, transverse and wall-normal velocity components in *x, y, z*-direction, respectively and follows the relations (Eq. 3):

$$u(t) = \overline{u} + u', v(t) = \overline{v} + v', w(t) = \overline{w} + w' \quad (3)$$

where the time-averaged velocity components are $\overline{u}, \overline{v}, \overline{w}$ and velocity fluctuations are u', v', w'. The time-averaged stream-wise, transverse and wall-normal mean velocities and root-mean-square velocity components σ_u, σ_v and σ_w are defined as follows Eqs. (4-9):

$$\overline{u} = \frac{1}{N}\sum_{i=1}^{N} u_i \quad (4)$$

$$\overline{v} = \frac{1}{N}\sum_{i=1}^{N} v_i \quad (5)$$

$$\overline{w} = \frac{1}{N}\sum_{i=1}^{N} w_i \quad (6)$$

$$\sigma_u = \sqrt{\frac{1}{N}\sum_{i=1}^{N}(u_i - \overline{u})^2} \quad (7)$$

$$\sigma_v = \sqrt{\frac{1}{N}\sum_{i=1}^{N}(v_i - \overline{v})^2} \quad (8)$$

$$\sigma_w = \sqrt{\frac{1}{N}\sum_{i=1}^{N}(w_i - \overline{w})^2} \quad (9)$$

The Reynolds shear stress at the measuring point is obtained as follows Eqs. (10-12):

$$\tau_{xz} = -\rho\overline{u'w'} = -\rho\frac{1}{N}\sum_{i=1}^{N}(u_i - \overline{u})(w_i - \overline{w}) \quad (10)$$

$$\tau_{xy} = -\rho\overline{u'v'} = -\rho\frac{1}{N}\sum_{i=1}^{N}(u_i - \overline{u})(v_i - \overline{v}) \quad (11)$$

$$\tau_{yz} = -\rho\overline{v'w'} = -\rho\frac{1}{N}\sum_{i=1}^{N}(v_i - \overline{v})(w_i - \overline{w}) \quad (12)$$

where: *N* is the total number of observations at each computing point and ρ is the density of fluid. Further, the results of mean velocities, intensities and shear stresses are normalized by the friction velocity (u_*). Therefore the above equations are recast and given as follows (Eq. 13):

$$\begin{aligned} &\hat{u} = \overline{u}/u_*,\ \hat{v} = \overline{v}/u_*,\ \hat{w} = \overline{w}/u_*, \\ &u^+ = \sigma_u/u_*, v^+ = \sigma_v/u_*, w^+ = \sigma_u/u_*, \\ &uw^+ = \overline{u'w'}/u_*^2, uv^+ = \overline{u'v'}/u_*^2, vw^+ = \overline{v'w'}/u_*^2 \end{aligned} \quad (13)$$

The normalized mean velocity components ($\hat{u} = \overline{u}/u_*$, $\hat{v} = \overline{v}/u_*$ and $\hat{w} = \overline{w}/u_*$), stream-wise turbulence intensity (u^+), bottom-normal turbulence intensity (w^+) and Reynolds shear stress (uw^+) over the flat surface are plotted all together for both Reynolds numbers in Fig. 3. The results over the plane bottom wall are in good agreement with the previous researchers (Nezu and Rodi, 1986; Nezu and Nakagawa, 1993). The friction velocity (u_* = 1.34 cm/s) is considered from the log-law (Schlichting, 1960) such as (Eq. 14):

$$\hat{u} = 1/\kappa \ln(z/z_0) + 5.5 \quad (14)$$

where: κ (= 0.4) and z_0 (= 0.0014 cm) are the von-Karman constant and equivalent bed roughness respectively satisfying good match with regression co-efficient $R^2 = 0.96$. To confirm the fully developed flow at the test section, two experiments were conducted at three different locations in the downstream direction of center-line of the flume and shown in Fig. 3. There are no significant changes observed in the turbulence characteristics such as time-averaged mean velocities in three directions and turbulent intensities, Reynolds shear stresses in stream-wise and bottom-normal directions for both Reynolds numbers over the test sections. The results on the flat surface are in good agreement with earlier study (Nezu and Rodi, 1986).

Literature suggests that the erosion process of cohesive sediment depends and is controlled by mechanical and physical properties (Debnath et al., 2007; Barman et al., 2019b; Roy et al., 2019; Das et al., 2019). Moreover, the cohesive sediment erosion and entrainment are highly dependent on the shear stress and the physicochemical properties of cohesive sediments (Ledden et al., 2004). Thereby, the primary mechanism that causes detachment or the initiation of the sediment in the flowing water includes the parameter such as velocity, intensity and the boundary shear stress (Jain and Kothyari, 2009). However, an empirical formula is proposed to determine the erosion rate E_r based on stepwise increment of bed shear stress following liner erosion formula (Sanford and Maa, 2001) (Eq. 15):

$$E_r = \rho_b \alpha(\tau_b - \tau_c)e^{-\gamma\alpha(t-t_0)} \quad (15)$$

where: ρ_b is the bulk density of the sediment sample, α is a constant, τ_b is the applied bed shear stress; τ_c is the critical shear stress; $\gamma = {}_{d\tau_c/dz}$ where z is the height with an arbitrary origin; t_0 is the time at which new stress is applied.

Moreover, it is pertinent from the experimental works of Sanford and Maa (2001) and of Ledden et al. (2004) that the critical shear stress for the cohesive sediment varies with amount of clay-sand proportion.

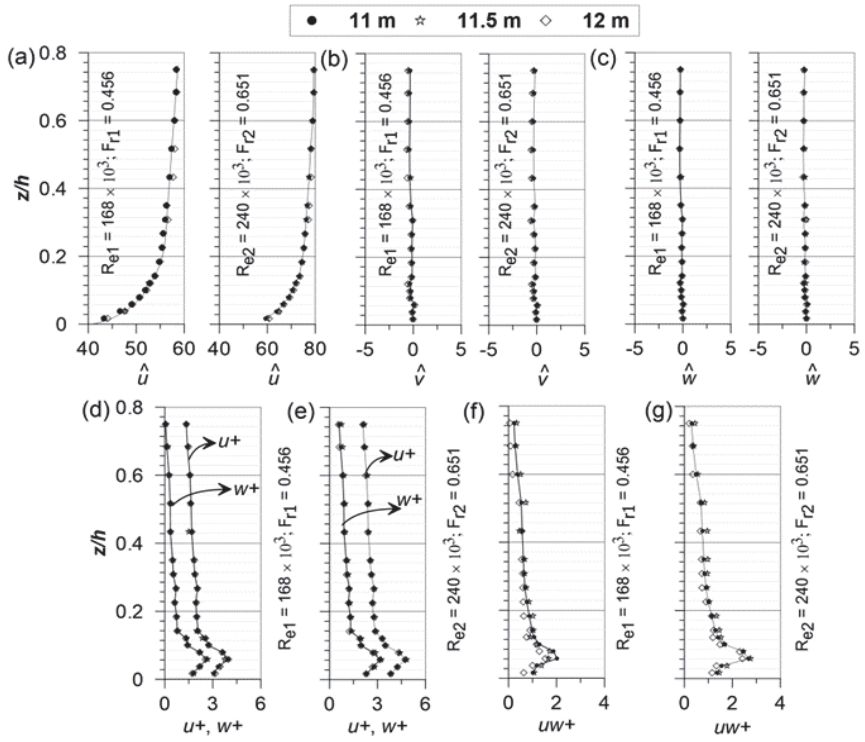

Fig. 3. (a) represents profiles of stream-wise, (b) transverseand (c) bottom-normal mean velocities $(\hat{u},\ \hat{v}$ and $\hat{w})$; (d, e) shows stream-wise and bottom-normal turbulence intensities ; and (f, g) signifies Reynolds shear stress based on present measurements on plane bed for both Reynolds numbers(Re1 and Re2) and at three stream-wise locations (11 m, 11.5 m and 12 m)

However, the present experiment could not verify such behaviour as it has been carried out using a single sediment type for different Reynolds number. Critical shear stress depends on the different parameters such as cohesive sediment viscosity, anchoring force, relative water content etc. Moreover, the comparative study (Taki, 2000) on the relation between non-dimensional mud viscosity and critical shear stress suggests that the critical shear stress may be varying with different clay composition and flow parameters. This experimental study is focus on the turbulence statistics on bank erosion. Thus, we did several initial test experiments with the same cohesive sediment composition used in this study. The results from the test run depict that after a normalized shear stress value (≈ 0.54) the sediment particle of cohesive bank starts to erode.

In this particular study we have obtained this stress as critical shear stress. Further, the erosion rates are initially high which with temporal evolution decreases and reach a steady state condition where the critical shear stress reduces (Das et al., 2019). In the present experiment the turbulence measurements were carried out when the undercut reached a steady state condition showing negligible erosion rate, to get a better understanding of the turbulence parameter within the undercut. Information congregated from the previous literature revealed that this particular investigation doesn't exist. For better engineering practices and river bank protection measurements this study would be a practical use for civil engineers and river geomorphologist. Thus, in the following sections the turbulence parameters such as mean velocity, turbulent intensities, Reynolds shear stress, turbulent kinetic energy, bursting events, time scale occurrence of ejection-sweep events and probability density function have been studied.

3.1. Mean velocities

Normalized stream-wise, transverse and bottom-normal mean velocities are plotted in Figs. 4 (a-c) respectively against normalized longitudinal distances (x/h) for three different flow depths, z/h = 0.141, 0.35 and 0.5 for both Reynolds numbers, R_e = 168000 and 240000. The normalized mean velocities before the erosion (i.e., at the plane bank) at z/h = 0.5 are shown in Figs. 4 (a-c) to compare it with the eroded side wall. The values of mean velocity significantly reduced at the near bottom bank flow depths, z/h = 0.141 and 0.35 in comparison with that of the upper depth, z/h = 0.5. The normalized profiles of stream-wise, transverse and bottom-normal mean velocity for the depth z/h = 0.5 are almost similar to the corresponding profiles of mean velocity before the erosion at level z/h = 0.5. It is clearly seen from Fig. 4a that the stream-wise mean velocity profiles are coincided for the depths, z/h = 0.141 and 0.35 for the Reynolds number, R_e = 168000; while the prominent variation of mean velocity profiles for these two flow depths is observed for the Reynolds number, R_e = 240000.

The stream-wise mean velocity at z/h = 0.5 seems not to change for R_{e1} = 168000 or even to slightly increase for R_{e2} = 240000 in some stream-wise regions compared to the profiles before erosion. It is evident from Figs. 4 (b, c) that the negative transverse and bottom-normal mean velocities exist at the eroded region of the side wall bank which signifies the occurrence of flow separation and recirculation in the undercut form by erosion. Furthermore, the transverse and bottom-normal mean velocities for R_e = 240000 decrease slightly greater in comparison with those of the R_e = 168000 at the eroded region of bank wall.

3.2. Turbulence intensities

Normalized stream-wise, transverse and bottom-normal turbulence intensities are plotted in Figs. 5 (a-c) respectively against normalized longitudinal distances (x/h) for three different flow depths, z/h = 0.141, 0.35 and 0.5 for two Reynolds numbers, R_e = 168000 and 240000. Observation from Figs. 5 (a-c) shows an increase in turbulent intensities (stream-wise, transverse and bottom-normal) within the eroded region. It is also to be noted that the stream-wise intensity within the eroded region is higher in magnitude as compared to transverse and bottom-normal intensities, which is true for both Reynolds numbers. The values of normalized intensities in all three directions before the erosion are significantly lower. The normalized stream-wise, transverse and bottom-normal turbulence intensities (Figs. 5 (a-c)) profiles at three levels, z/h = 0.141, 0.35 and 0.5 for the two Reynolds numbers also illustrate an increase in intensities within the eroded region as compared to intensities profile in the non-eroded region. However, the values of intensities reduce significantly at z/h = 0.141 and 0.5 in comparison with those of z/h = 0.35. Thus, the turbulence intensity at the mid-depth is generally higher than that of the near bottom flow depth and upper depth. Moreover, the variation of intensity profile observed for R_e = 240000 is more prominent than R_e = 168000.

The increased turbulent intensity resulted in the generation of higher potential for the dislodgement and suspension of the cohesive sediment particles from the bank face. This higher magnitude of turbulent intensity resulted in the dislodgement of larger chunk of sediment particles from the bank face as compared to the lower intensity magnitude. Of note, the lower turbulence intensity leads to settlement of sediment.

3.3. Reynolds shear stress

Normalized Reynolds shear stresses (uw^+), (uv^+) and (vw^+) are plotted in Figs. 6 (a-c) respectively against normalized longitudinal distances (x/h) for three different flow depths, z/h = 0.141, 0.35 and 0.5 for two Reynolds numbers, R_e = 168000 and 240000. Large positive Reynolds stress is formed along the interface between the mainstream and undercut region.

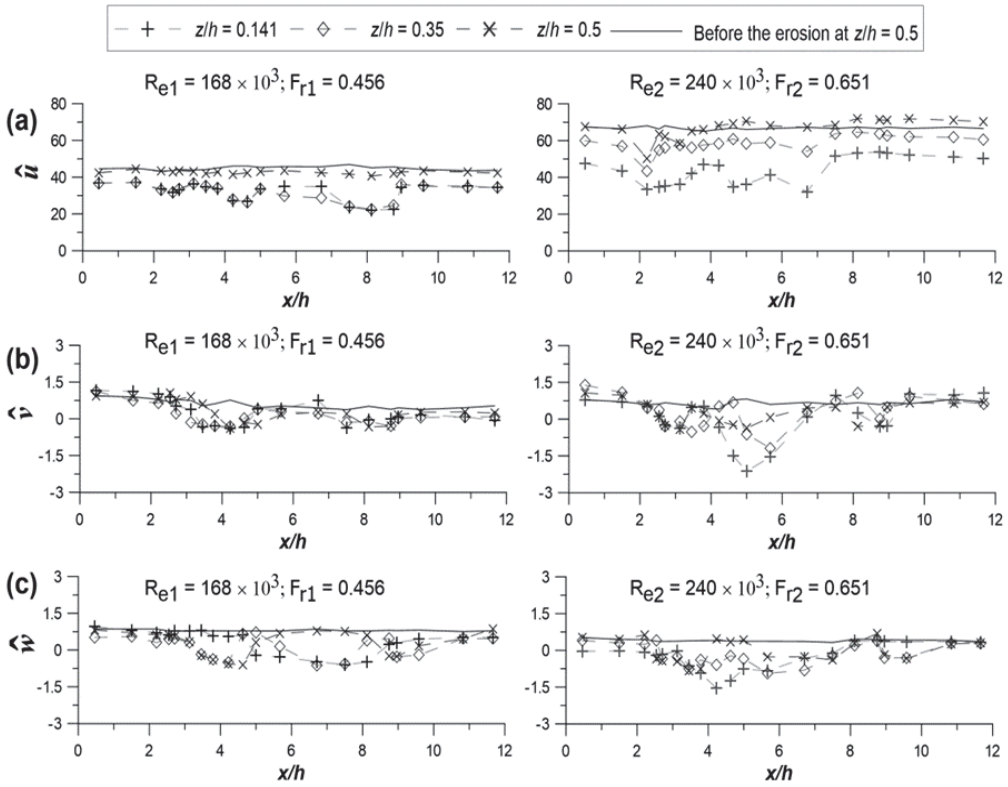

Fig. 4. Normalized mean velocities ((*a*) $\hat{u} = \overline{u}/u_*$, (b) $\hat{v} = \overline{v}/u_*$ and (c) $\hat{w} = \overline{w}/u_*$) profiles against the longitudinal distance (x/h) at three different flow depths, z/h = 0.141, 0.35 and 0.5 for two Reynolds numbers respectively. Solid linerepresents the normalized mean velocities before the erosion at z/h = 0.5

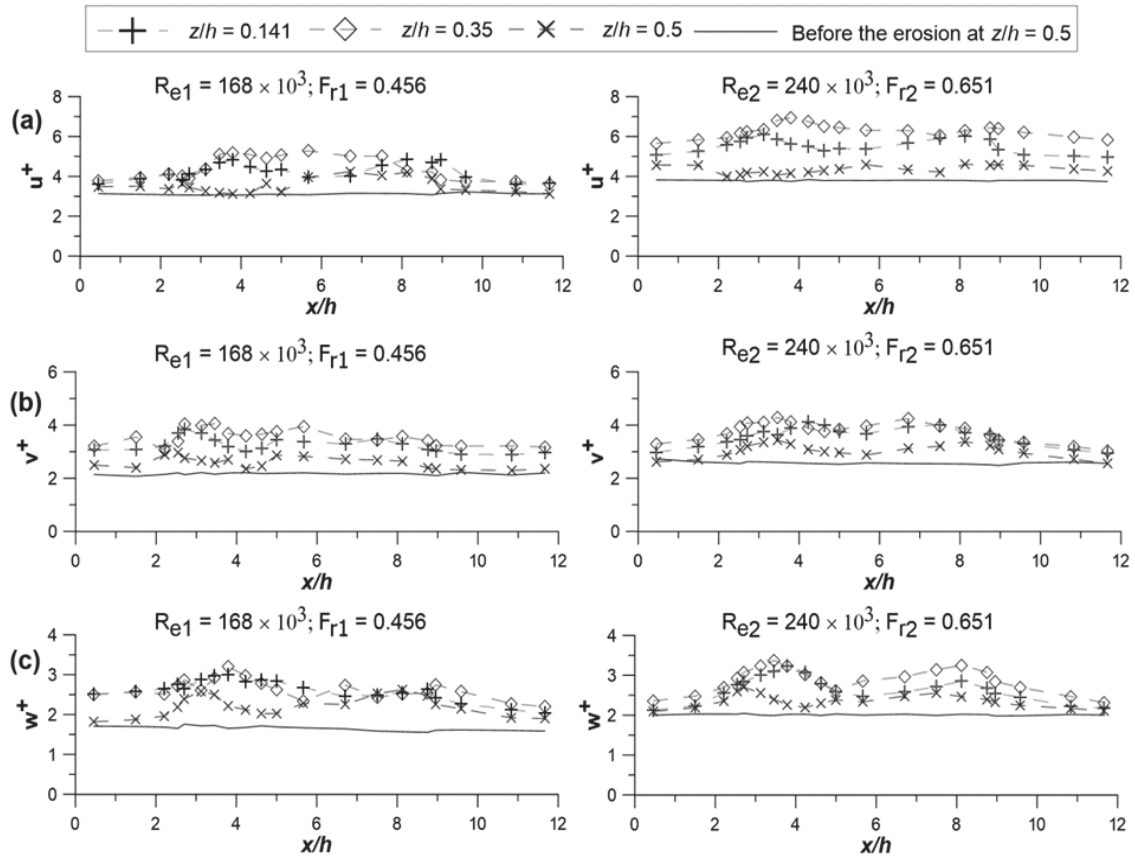

Fig. 5. Normalized turbulent intensities ((a) u^+, (b) v^+, (c) w^+) profile alongthe stream-wise direction at three different level z/h = 0.141, 0.35 and 0.5 fortwo Reynolds numbers respectively. Solid line represents the normalized turbulence intensities components along stream-wise direction before the erosion at z/h = 0.5

As a result, the enhancement of the erosion process was observed which may due to introduction of shear stresses. The width of stress zones increases in the stream-wise direction, irrespective of the vertical elevation. Furthermore, these zones are also modulated with the flow Reynolds number. Possibly, the increment of stress zone in the stream-wise direction results in enlargement of undercut in the horizontal compare to vertical direction. Thereby increasing the volume of the undercut, this was observed in the present experiment.

Moreover, the magnitude of uw^+ is higher as compared to uv^+ and vw^+ for both Reynolds numbers. It is evident from Figs. 6 (a-c) that the Reynolds shear stresses at three levels, z/h = 0.141, 0.35 and 0.5 for the two Reynolds numbers also demonstrated an increase in Reynolds shear stresses within the eroded region as compared to Reynolds stresses profile in the non-eroded region. It is noted that the shear stress at the mid-depth(z/h = 0.35) is slightly higher than that of the near bottom flow depth (z/h = 0.141) and upper depth (z/h = 0.5). It is seen from Figs. 6 (a-c) that the variation of Reynolds shear stresses profile for R_e = 240000 is more prominent than R_e = 168000. However, the Reynolds shear stresses value at the upper depth for both Reynolds numbers are minimum and almost coincides with the Reynolds shear stresses profile before the erosion.

3.4. Turbulent kinetic energy

The turbulent kinetic energy (TKE) value is primarily used to evaluate the extent of fluid mixing in a turbulent flow. The turbulence kinetic energy can be given as (Eq. 16a):

$$TKE(k) = 0.5\left(u'^2 + v'^2 + w'^2\right) \tag{16a}$$

Normalized TKE (k^+) is defined as following (Eq. 16b):

$$k^+ = k/u_*^2 \tag{16b}$$

Normalized turbulent kinetic energy (k^+) for both Reynolds numbers (R_{e1} and R_{e2}) are estimated from Eq. 16b for the centre location of eroded regions (Fig. 1c, 1d) of the bank wall at three different flow depths, z/h = 0.141, 0.35 and 0.5 and plotted in Fig. 7 (a, b). The normalized TKE (k^+) for pre-erosion at z/h = 0.5 is also included in Fig. 7 (a, b). The centre locations of first, second and third eroded region for R_{e1} were found x/h = 2.5, 4.2 and 8.2 respectively; similarly for R_{e2}, it was x/h = 2.3, 2.5 and 6.7 respectively. It is observed from Fig. 7 that the magnitude of k^+ is higher for the Reynolds number, R_{e2} = 240000 in comparison with that of the Reynolds number, R_{e1} = 168000.

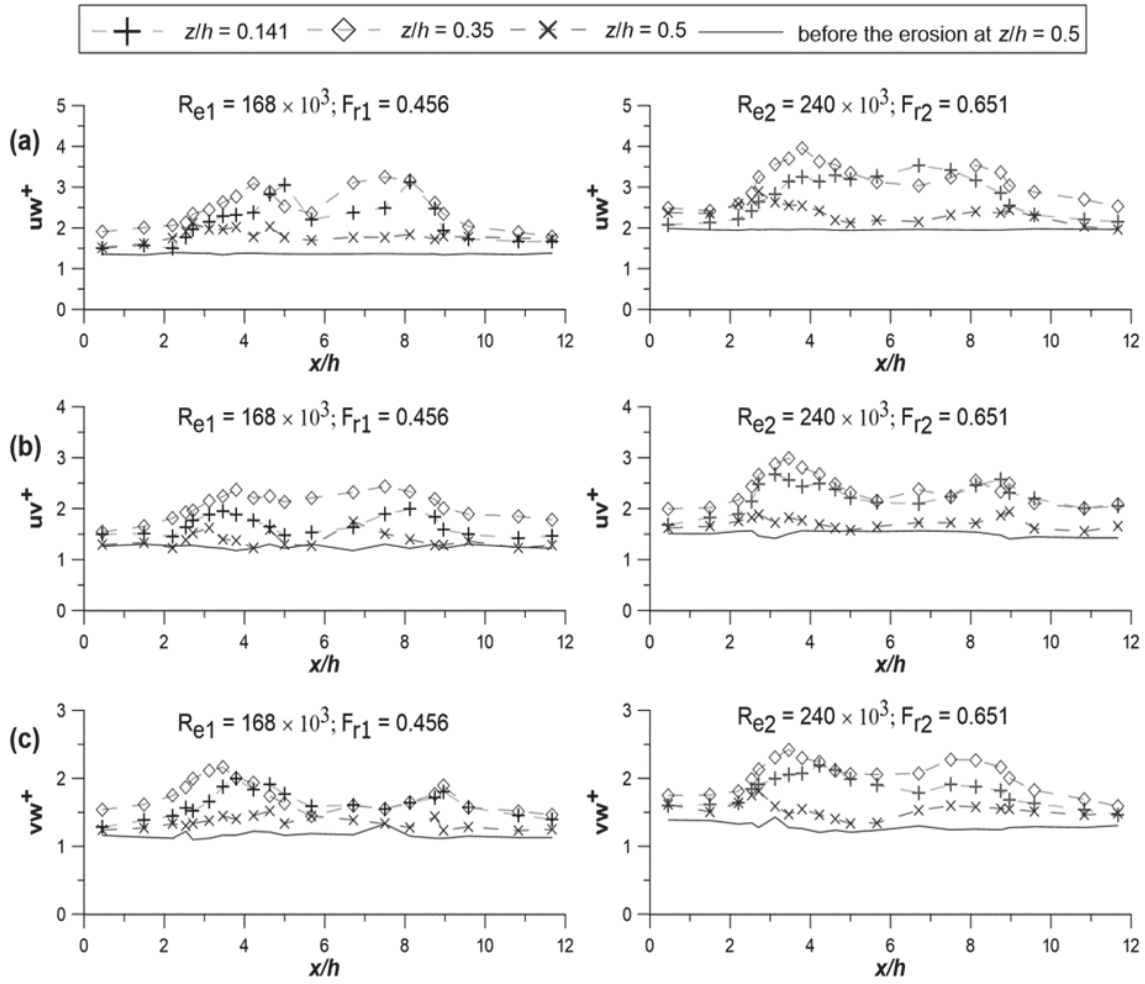

Fig. 6. Normalized Reynolds shear stresses ((a) uw^+, (*b*) uv^+, (c) vw^+) alongthe stream wise direction at three different level *z*/*h* = 0.141, 0.35 and 0.5for two Reynolds numbers respectively. Solid line represents the normalized Reynoldsshear stresses along stream-wise direction before the erosion at *z*/*h* = 0.5

It is evident from Figs. 7 (a, b) that the values of k^+ increases due to eroded side bank for all these flow depths compared to before eroded side wall at *z*/*h* = 0.5 for both Reynolds numbers. Furthermore, the values of k^+ are maximum for the flow depth, *z*/*h* = 0.35 compared to other flow depths. However, the values of k^+ are nearly 29-43% and 47-55% greater for *z*/*h* = 0.35 compared to before eroded bank for the respective Reynolds number, R_e = 168000 and 240000. A high magnitude of k^+ is also observed in scour region. Further, values of k^+ increases with increasing discharge at the near flow vertical bank region (McBride et al., 2007).

Therefore, it is noted that the increasing k^+ is observed at the core region of the bank which may probably due to the influence of adverse pressure gradient near the bank flow and the retarded fluids particles cannot withstand and penetrate too far into the region of increased pressure owing to their small kinetic energy.

3.5. Quadrant analysis

Bursting phenomenon such as ejection-sweep event plays a key role for erosion, deposition, and transport of sediment which is important in bank erosion problem. The quadrant analysis was introduced (Willmarth and Lu, 1972) to quantify the usefulness of sign of turbulent velocity fluctuations and their contribution into the Reynolds shear stress in *xz*-plane. In the quadrant analysis, the velocity fluctuations are categorized with four quadrants namely first (Q1), second (Q2), third (Q3) and fourth (Q4) quadrant. The first quadrant Q1 $(u'>0, w'>0)$ corresponds to the outward interaction event. Similarly, second quadrant Q2 $(u'<0, w'>0)$, third quadrant Q3 $(u'<0, w'<0)$ and fourth quadrant Q4 $(u'>0, w'<0)$ corresponds to ejections, inward interactions and sweeps event respectively (Lu and Willmarth, 1973; Nezu and Nakagawa, 1993).

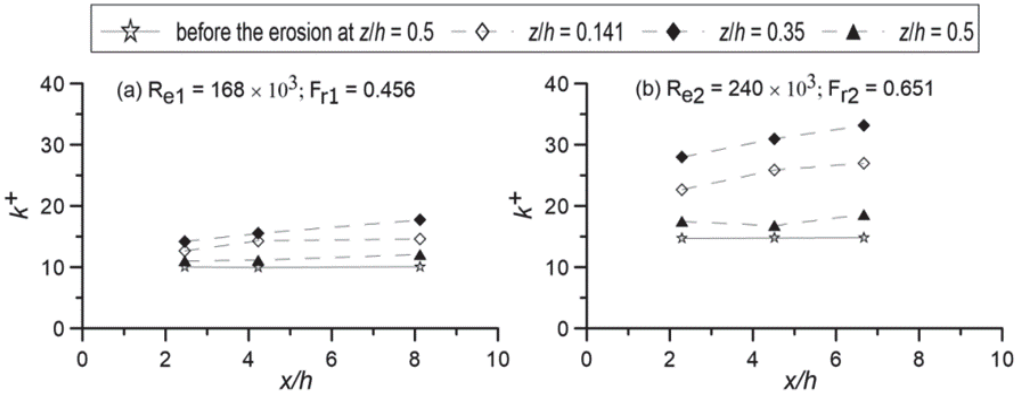

Fig. 7. Normalized turbulent kinetic energy (k^+) at the centre location (x/h) of the eroded side wall bank for three different flow depths, z/h = 0.141, 0.35 and 0.5 and before the erosion at z/h = 0.5 for (a) Reynolds number, R_{e1} = 168000 and (b) R_{e1} = 240000 respectively

The most important events are ejection and sweep, transporting low and high momentum fluid in upward and downward directions, respectively and these events yield turbulent energy; whereas the inward and outward interactions provided energy dissipation (Pope, 2000). The normalized Reynolds shear stress distribution of uv^+, uw^+ and vw^+ has been shown in Fig. 6 for before and after eroding of the bank. Among all stress distributions, the Reynolds shear stress, uw^+ has been considered for quadrant analysis. The contribution of bursting events to the shear stress at any point from quadrant *i*, excluding a hyperbolic hole region *H*, is defined as follows (Eq. 17):

$$\left(u'w'\right)_{i,H} = \lim_{T\to\infty}\frac{1}{T}\int_0^T u'(t)w'(t)I_{i,H}\left[u'(t),w'(t)\right]dt \qquad (17)$$

where: the indicator function $I_{i,H}$ is expressed as follows (Eq. 18):

$$I_{i,H}(u'w') = \begin{cases} 1, & \text{if (u'w') is in the ith quadrant and} \\ \text{if} & |u'w'| \geq H\,|\overline{u'w'}| \\ 0, & \text{otherwise} \end{cases} \qquad (18)$$

The stress fraction in *i*-th quadrant is as follows (Eq. 19) (Barman et al., 2017; Raupach, 1981).

$$S_{i,H} = \frac{(u'w')_{i,H}}{\overline{u'w'}} \qquad (19)$$

To consider the strength of turbulent signals, the time fraction, $T_{i,H}$ is calculated using the average of $I_{i,H}$ and it is written as (Eq. 20):

$$T_{i,H} = \overline{I_{i,H}\left(u',w'\right)} = \lim_{x\to\infty}\frac{1}{T}\int_0^T I_{i,H}\left(u'(t),w'(t)\right)dt \qquad (20)$$

The contributions of $\left|S_{i,H}\right|$ to the stress are framed against the hole size *H* for each of the four quadrants for two Reynolds numbers in Fig. 8 and Fig. 9 at the location V1, V2, V3 and V4 for two different levels (z/h = 0.141, 0.35). Here, the location V1 represents the measured data at the bank face (non-eroded region) and V2, V3 and V4 represent three eroded regions as shown in Fig. 1 for two Reynolds numbers. In general, it is evident from both Figs. 8 and 9 that the contributions of ejection and sweep ($Q2$ and $Q4$) to the Reynolds shear stress are more dominant than that of the outward and inward interactions ($Q1$ and $Q3$) at the measurement locations V1-V4 for R_e = 168000 and 240000 respectively. Furthermore, it is perceived from Figs. 8-9 that the all these four events are almost equally contributed for non-eroded region (location V1, at x/h = 6) for the flow depth, z/h = 0.141 compared with z/h = 0.35. However, contributions of all these events are greater for z/h = 0.35 in comparison with the flow depth, z/h = 0.141 for both Reynolds numbers at the eroded region of bank face (locations V2, V3, and V4). The contributions of ejection and sweep ($Q2$ and $Q4$) to the Reynolds shear stress at the bank face are dominated signifying the initiation of the erosion process. However, for R_e = 168000 at the first eroded region (location V2), the contributions of inward and outward interaction events are significantly less for the near-bed region (z/h = 0.141) compare with those of upper flow depth region, z/h = 0.35.

The contributions of sweep events are nearly 50% and the ejection events contributions are nearly 40% greater for z/h = 0.35 compared to z/h = 0.141. Thus, the sediments are dislodged due to ejection events and are carried and transported due to sweep events. While, at the last eroded region (Fig. 8; location V4), sweep events are equally contributed for both flow depths for R_e = 168000. Furthermore, at location V2 (Fig. 9) it is observed that the contribution of the ejection and sweep events is almost equal i.e., $S_{2,0} \approx S_{4,0} \approx 0.82$ for z/h = 0.14; while, at z/h = 0.35, $S_{2,0} \approx S_{4,0} \approx 0.98$ for hole size, H = 0. Thus, it may signify that the transport process is symmetric on the eroded bank face.

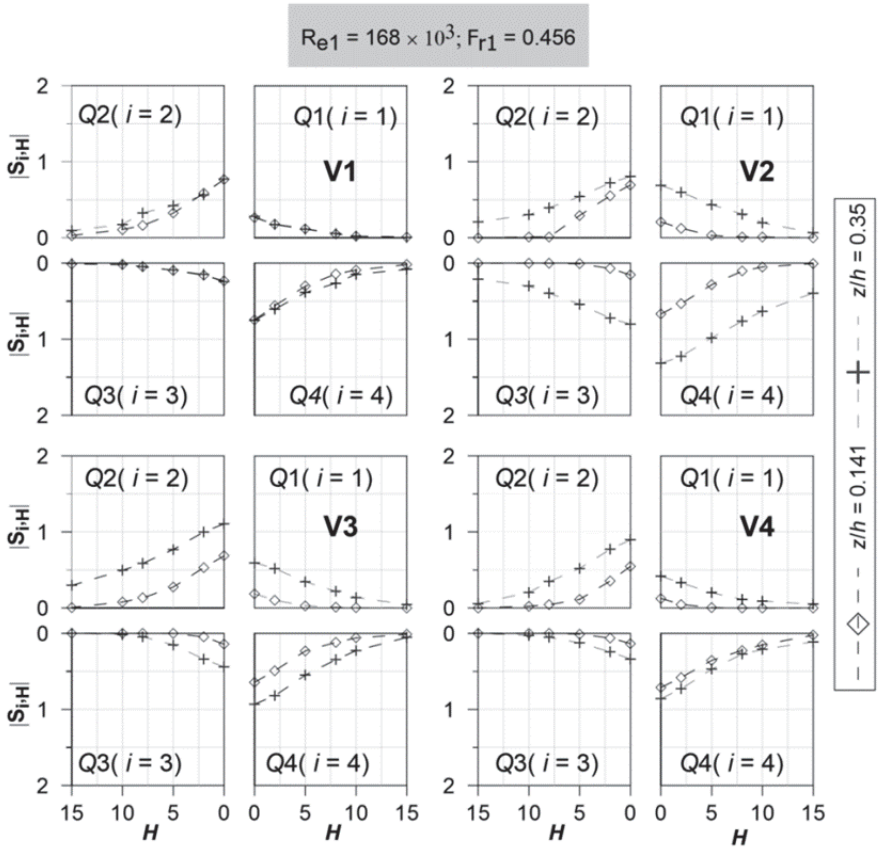

Fig. 8. Represents the stress fraction, $|S_{i,H}|$ against hole size *H*, measured at *z/h* = 0.141 and 0.35 for vertical V1, V2, V3 and V4

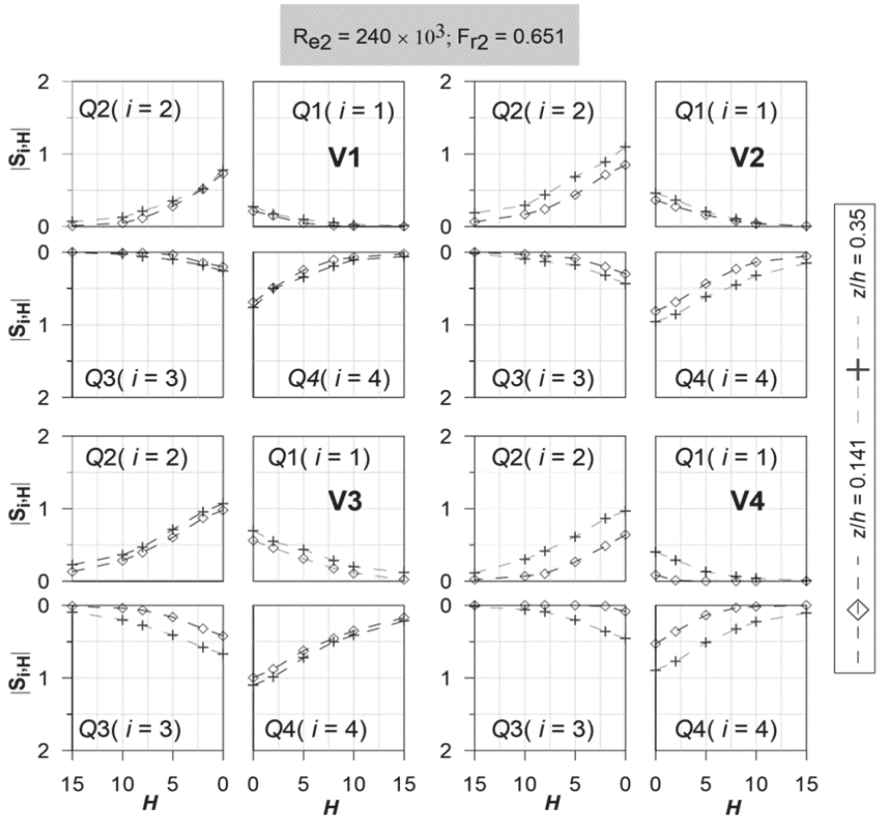

Fig. 9. Represents the stress fraction, $|S_{i,H}|$ against hole size *H*, measured at *z*/*h* = 0.141 and 0.35 for vertical V1, V2, V3 and V4

Also, outward and inward interaction events are symmetric for each contributing equal i.e., $S_{1,0} \approx S_{3,0} \approx 0.33$ for $z/h = 0.141$; whereas at $z/h = 0.35$, $S_{1,0} \approx S_{3,0} \approx 0.45$ for $H = 0$ and each diminishing to contribute when $H \geq 8$. Similar findings were observed by Raupach (1981).

3.6. Time-scale of occurrence of ejection-sweep events

Distributions of the mean time interval for the occurrence of ejection and sweep cycles against hole size, H for measuring verticals V1, V2, V3,and V4 are shown in Figs. 10-11 at two different levels (z/h = 0.141 and 0.35) for two Reynolds numbers respectively. The occurrence of ejection and sweep time intervals are measured from the fluctuating velocity in the flow field for the hole size H with filtering the data using the condition $|u'w'| \leq H\overline{|u'w'|}$.

The mean time scales of ejection and sweep cycle occurrences against varying hole size H in order to the velocity data of 180 s measured at the fixed rate of 40 Hz for each vertical (Barman et al., 2017; Debnath et al., 2012). In general, it is observed from Figs. 10-11 that the mean time interval of occurrence of ejection-sweep events is significantly largest for the near-bed region flow depth $z/h = 0.141$ in comparison to that of the flow depth, $z/h = 0.35$ for the higher value of H. It is observed from Figs. 10-11 at location V1, the mean time interval for the occurrence of the ejection-sweep events are significantly less for no eroded bank face (location V1) in comparison to that of the locations V2, V3 and V4 cases.

It is evident from Figs. 10-11 that all the distributions of the time interval for the occurrence of the ejection and sweep show concave up with positive increasing slops for both flow depths at the measuring points of eroded and non-eroded bank face for R_e = 168000 and 240000 respectively. It is noted from Figs. 10 and 11 that the mean time interval for the occurrence of the ejection and sweep events are identical up to hole size ($H = 2$) for these flow depths. The mean time interval for the occurrence of the ejection is nearly 70% largest for the depth, $z/h = 0.141$ compared to $z/h = 0.35$ for the second eroded region of bank face (Fig. 10; location V3). However, the mean time interval for the occurrence of the sweep is about 8-15% greater in comparison with the time interval for the occurrence of the ejection for R_e = 168000. Similar nature is observed for the higher Reynolds number (R_e = 240000).

3.7. Probability density function (PDF)

The distribution pattern of probability density function (PDF) of velocity fluctuations is important to understand the nature of the velocity time series (e.g., Tennekes and Lumley, 1972). Figs. 12 (a, b) shows the PDF of stream-wise and wall-normal velocity components at the eroded and non-eroded region of bank face (locations V1, V2, V3,and V4) studied herein for two Reynolds numbers, R_e = 168000 and 240000 respectively. It is clear from Figs. 12 (a, b) that the distribution of PDF of lateral velocity fluctuations (v') shows narrow distributions with higher peaks than the stream-wise velocity fluctuations (u').

The highest values of u' are almost similar at all these measuring locations within the maximum eroded zone as well as the plane bank face (upstream and downstream of the bank undercut). However, the PDF distribution for v' are clearly distinguishable and it shows that large probability density of v' in the eroded zone than no eroded zone. The flatter distribution of PDF of u' signifies that large-scale stream-wise velocity fluctuation is frequent the near bank face. It may be due to the near bank wall shear stress, which acts as a reagent for producing vortices (large scale stream-wise velocity fluctuations) from the bank face and these vortices enhance the random velocity fluctuating scale.

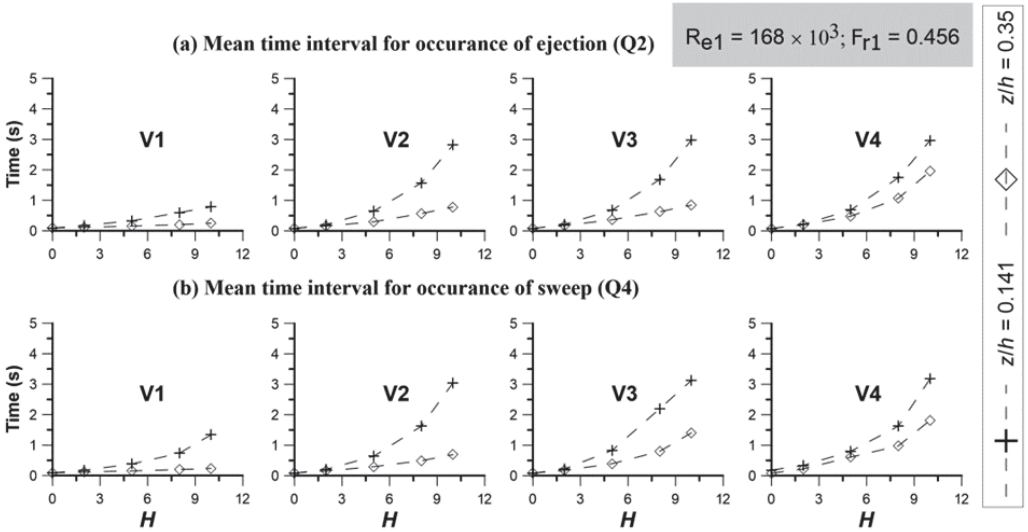

Fig. 10. Represents the distributions of mean time interval for occurrence of (a) ejection and (b) sweep events against hole size (H) for verticals V1, V2, V3 and V4

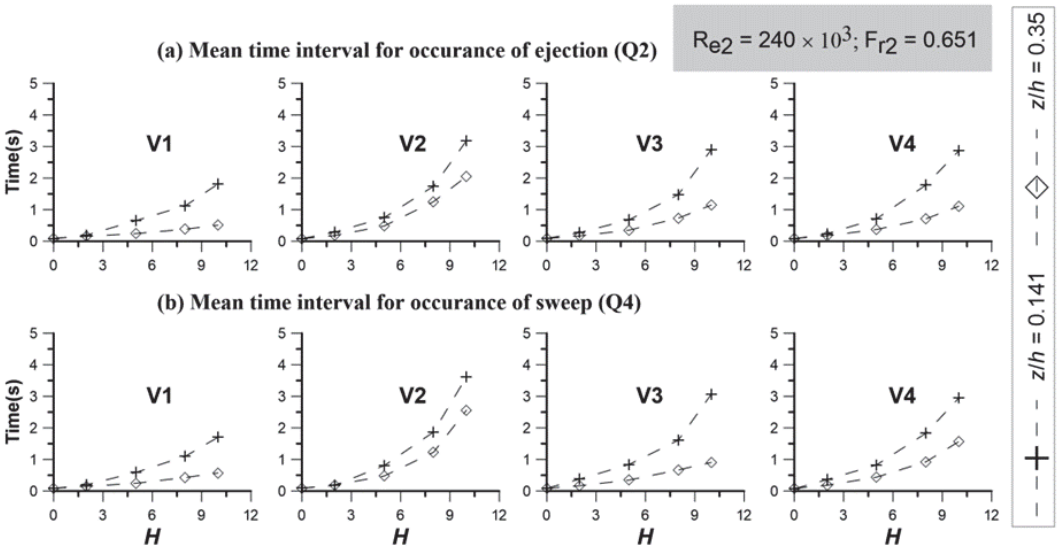

Fig. 11. Distributions of mean time interval for occurrence of (a) ejection and (b) sweep events against hole size (H) for verticals V1, V2, V3 and V4

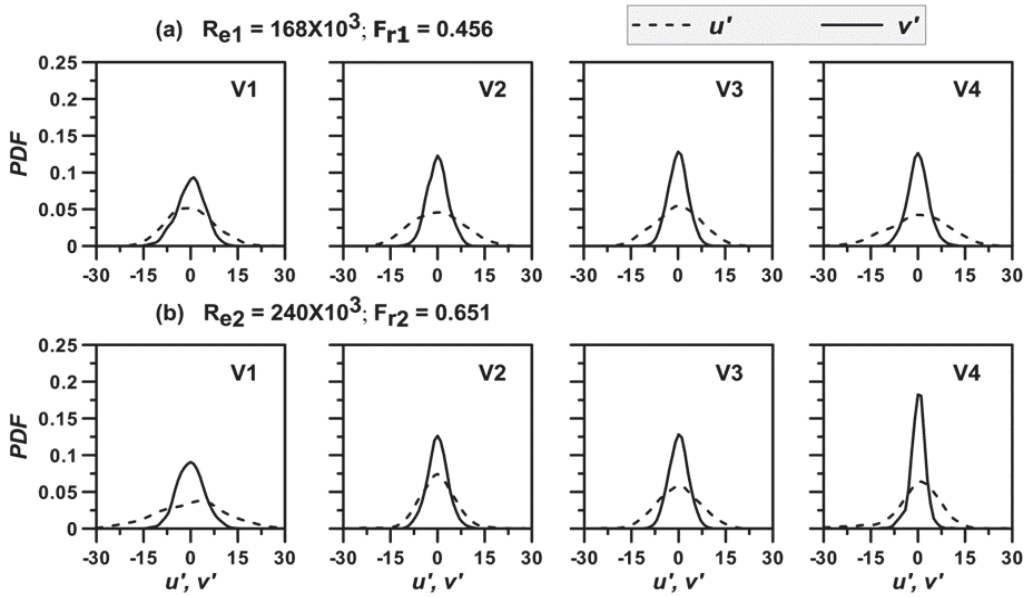

Fig. 12. Distributions probability density function of stream-wise and bottom-normal velocity components at the locations V1, V2, V3 and V4 for (a) R_e = 168000 and (b) R_e = 240000

Similar consequences are found for higher Reynolds number R_e = 240000. Thus, it is interesting to note that two types of features of velocity fluctuations distribution of the random fluctuating flow field occur within the bank undercut at the upstream and downstream locations of the eroded zone: (a) the concentration of smaller scale fluctuations of the lateral velocity component increases near the downstream side of the eroded zone; (b) large-scale fluctuations of stream-wise velocity component are added to the fluctuations distribution near the bank face.

4. Conclusions

In nature, river bank or any other stream bank erosion and formation of irregular undercut are caused by bank failure which has a direct effect on environmental and social issues. The results of the present study may be of an area of great concern to environmentalists and river planners to understand the flow behavior for minimizing the erosion process. The main results from the study are detailed as:

- The normalized stream-wise, transverse and bottom-normal mean velocities decrease near the eroded region of bank face in comparison with the non-eroded bank surface. Negative transverse and bottom-normal mean velocities are responsible for the occurrence of flow separation and recirculation.
- The normalized turbulence intensities and Reynolds shear stress increase within the eroded region. Further, the turbulence intensity at the mid-depth is higher than those of the near bottom flow depth and upper depth.

• The magnitude of turbulence kinetic energy is higher for high Reynolds number compared to other low Reynolds numbers. Moreover, the values of TKE are maximum for the flow depth, $z/h = 0.35$ compared to other flow depths.

• Contributions of ejections and sweeps to the Reynolds shear stress are much higher than those of outward and inward interactions for measuring locations of eroded bank region.

• The average time intervals for the occurrence of the ejection and sweep in relation to the employed threshold show concave up for all the flow depths at the measuring points of eroded and non-eroded bank face for both Reynolds numbers.

• The distribution of PDF of lateral velocity fluctuations shows narrower compared to the stream-wise fluctuations. Furthermore, the PDF distribution of u' is flatter and it confirms the large-scale stream-wise velocity fluctuations dominate the near bank face.

Acknowledgments

The authors would like to acknowledge the Department of Science and Technology, Government of India for financial support for this research (Contact No. EMR/2015/000266).

References

Barman K., Debnath K., Mazumder B.S., (2016), Turbulence between two inline hemispherical obstacles under wave-current interactions, *Advances in Water Resources*, **88**, 32-52.

Barman K., Debnath K., Mazumder B.S., (2017), Higher-order turbulence statistics of wave-current flow over a submerged hemisphere, *Fluid Dynamics Research*, **49**, 025504.

Barman K., Debnath K., Mazumder B.S., (2019a), Turbulence over chains of hemispherical ribs under waves in a current, *Water Resources Research*, **55**, 55-75.

Barman K., Roy S., Das V.K., Debnath K., (2019b), Effect of clay fraction on turbulence characteristics of flow near an eroded bank, *Journal of Hydrology*, **571**, 87-102.

Best J.L., (1993), *On the Interactions Between Turbulent Flow Structure, Sediment Transport and Bedform Development: Some Considerations from Recent Experimental Research*, In: *Turbulence: Perspectives on Flow and Sediment Transport*, Clifford N.J., French J.R., Hardisty J. (Eds.), Wiley, Chichester, 61-92.

Cao D.P., Chiew Y.M., (2014), Suction effects on sediment transport in closed-conduit flow, *Journal of Hydraulic Engineering*, **140**, 04014008.

Chanson H., Trevethan M., Koch C., (2007), Discussion of "turbulence measurements with acoustic doppler velocimeters" by Carlos M. Garcia, Mariano I. Cantero, Yarko Nirio and Marcelo H. Garcia, *Journal of Hydraulic Engineering*, **133**, 1283-1286.

Chen X., Chiew Y., (2004), Velocity distribution of turbulent open-channel flow with bed suction, *Journal of Hydraulic Engineering*, **130**, 140-148.

Das V.K., Roy S., Barman K., Debnath K., Chaudhuri S., Mazumder B.S., (2019), Investigations on undercutting processes of cohesive river bank, *Engineering Geology*, **252**, 110-124.

Debnath K., Nikora V., Elliott A., (2007), Stream bank erosion: in situ flume tests, *Journal of Irrigation and Drainage Engineering*, **133**, 256-264.

Debnath K., Chaudhuri S., (2010), Bridge pier scour in clay-sand mixed sediments at near-threshold velocity for sand, *Journal of Hydraulic Engineering*, **136**, 597-609.

Debnath K., Manik M.K., Mazumder B.S., (2012), Turbulence statistics of flow over scoured cohesive sediment bed around circular cylinder, *Advances in Water Resources*, **41**, 18-28.

Garcia C.M., Jackson P.R., Garcia M.H., (2006), Confidence intervals in the determination of turbulence parameters, *Experiments in Fluids*, **40**, 514-522.

Goring D.G., Nikora V.I., (2002), Despiking acoustic Doppler velocimeter data, *Journal of Hydraulic Engineering*, **128**, 117-126.

Grass A.J., (1971), Structural features of turbulent flow over smooth and rough boundaries, *Journal of Fluid Mechanics*, **50**, 233-255.

Hansda S., Barman K., Roy S., Debnath K., (2019), Quantification of turbulent eddies in time-space and frequency domain for wave-current combined flow over side-wall roughness, *Ocean Engineering*, **186**, 106080.

Huai W.X., Zhang J., Wang W.J., Katul G.G., (2019a), Turbulence structure in open channel flow with partially covered artificial emergent vegetation, *Journal of Hydrology*, **573**, 180-193.

Huai W.X., Zhang J., Katul G.G., Cheng Y.G., Tang X., Wang W.J., (2019b), The structure of turbulent flow through submerged flexible vegetation, *Journal of Hydrodynamics*, **31**, 1-20.

Jain R.K., Kothyari U.C., (2009), Cohesion influences on erosion and bed load transport, *Water Resources Research*, **45**, 1-17.

Katopodis C., (1996), *Ecohydraulics: Challenges and Opportunities with Fish and Fish Habitat*, Proc. of Ecohydraulics 2000, 2nd Int. Symp. on Habitat Hydraulics, INRS-Eau, Quebec, 555-578.

Ledden M., Van Kesteren W.G.M., Winterwerp J.C., (2004), A conceptual framework for erosion behaviour of sand-mud mixtures, *Continental Shelf Research*, **241**, 1-11.

Lu S.S., Willmarth W.W., (1973), Measurements of the structures of the Reynolds stress in a turbulent boundary layer, *Journal of Fluid Mechanics*, **60**, 481-571.

Maclean A.G., (1991), Open channel velocity profiles over a zone of rapid infiltration, *Journal of Hydraulic Research*, **29**, 15-27.

Maclean A.G., Willetts B.B., (1986), Measurement of boundary shear stress in nonuniform open channel flow, *Journal of Hydraulic Research*, **24**, 39-51.

Meijer D.G., Van Velzen E.H., (1999), *Prototype-Scale Flume Experiments on Hydraulic Roughness of Submerged Vegetation*, Proc. of the 28th Int. IAHR Conf., Graz, 1-8.

McBride M., Hession W.C., Rizzo D.M., Thompson D.M., (2007), The influence of riparian vegetation on near-bank turbulence: A flume experiment, *Earth Surface Processes and Landform*, **32**, 2019-2037.

Nezu I., Onitsuka K., (2001), Turbulent structure in partly vegetated open channel flows with LDA and PIV measurements, *Journal of Hydraulic Research*, **39**, 629-642.

Nezu I., Nakagawa H., (1993), *Turbulence in Open-Channel Flows*, CRC Press, Rotterdam, 1-293.

Nezu I., Rodi W., (1986), Open-channel flow measurements with a Laser Doppler anemometer, *Journal of Hydraulic Engineering*, **112**, 335-355.

Nikora V.I., Goring D.G., (1998), ADV measurements of turbulence: Can we improve their interpretation?, *Journal of Hydraulic Engineering*, **124**, 630-634.

Pope S.B., (2000), *Turbulent Flows*, Cambridge University Press, Cambridge, 1-771.

Raupach M.R., (1981), Conditional statistics of Reynolds stress in rough-wall and smooth wall turbulent boundary layers, *Journal of Fluid Mechanics*, **108**, 363-382.

Rao A.R.K., Sitaram N., (1999), Stability and mobility of sand bed channels affected by seepage, *Journal of Irrigation and Drainage Engineering*, **125**, 370-379.

Rao A.R.K., Sreenivasulu G., Kumar B., (2011), Geometry of sand-bed channels with seepage, *Geomorphology*, **128**, 171-177.

Roy S., Das V.K., Debnath K., (2019), Characteristics of intermittent turbulent structures for river bank undercut depth increment, *Catena*, **172**, 356-368.

Rutherford J.C., (1994), River mixing, *Journal of Fluid Mechanics*, **299**, 406-407.

Sanford L.P., Maa J.P.Y., (2001), A unified erosion formulation for fine sediments, *Marine Geology*, **179**, 9-23.

Shiono K., Knight D.W., (1991), Turbulent open-channel flows with variable depth across the channel, *Journal of Fluid Mechanics*, **222**, 617-646.

Smith C.R., (1996), *Coherent Flow Structures in Smooth-Wall Turbulent Boundary Layers: Facts*, *Mechanisms*, *And Speculation*, In: *Coherent Flow Structures in Open Channels*,Ashworth P.J., Bennett S.J., Best J.L., McClelland S.J. (Eds.), Wiley, Chichester, 1-39.

Singha A., Faruque M.A.A., Balachandar R., (2012), Vortices and large-scale structures in a rough open channel flow subjected to bed suction and injection, *Journal of Engineering Mechanics*, **138**, 491-501.

Thompson D., Wohl E., (1998), *Flume Experimentation and Simulation of Bedrock Channel Processes*, In: *Rivers over Rock: Fluvial Processes in Bedrock Channels*,Tinkler K.J., Wohl E.E. (Eds.), American Geophysical Union, Washington, DC, 279-296.

Taki K., (2000), *Critical Shear stress for Cohesive Sediment Transport*, In: *Coastal and Estuarine Fine Sediment Processes*, McAnally W.H., Mehta A.J. (Eds.), vol. III, 1st Edition, Elsevier Science, 53-61.

Tritton D.J., (1988), *Physical Fluid Dynamics*, 2nd Edition, Clarendon, Oxford University Press, Oxford, UK.

Tennekes H., Lumley J.L., (1972), *A First Course in Turbulence*, Cambridge University Press, Cambridge, 816-819.

Willmarth W.W., Lu S.S., (1972), Structure of the Reynolds stress near the wall, *Journal of Fluid Mechanics*, **55**, 65-92.

Wormleaton P.R., (1996), *Floodplain Secondary Circulation as a Mechanism for Flow and Shear Stress Redistribution in Straight Compound Channels*, In: *Coherent Flow Structures in Open Channels*, Ashworth P.J., Bennett S.J., Best J.L., McClelland S.J. (Eds.), Wiley, Chichester, 581-608.